

## A Code Comparison Exercise Based on the LMFBR Containment Experiment MARA-04

B.L. Smith

*Swiss Federal Institute for Reactor Research, CH-5303 Würenlingen, Switzerland*

C. Fiche, J. Louvet

*C.E.A., CEN Cadarache, DRNR, B.P. No. 1, F-13115 St. Paul-lez-Durance, France*

A. Zucchini

*ENEA, CRE "E. Clementel", Via Mazzini 2, I-40138 Bologna, Italy*

### ABSTRACT

A code comparison exercise is reported based on calculations performed for the LMFBR containment experiment MARA-04. Three codes are specifically involved in the study: SEURBNUK-EURDYN, CASSIOPEE, SIRIUS, but previously published results from a parallel ASTARTE calculation are also included in the comparison. The codes together form a representative cross-section of the numerical approaches adopted for containment analysis.

Particular attention is paid to the specification of the material constitutive laws, which include strain-rate dependent effects in some cases.

### 1. INTRODUCTION

In support of LMFBR safety analysis requirements in Europe a number of computer codes have been developed to help assess the structural integrity of primary containment closures under HCDA load conditions. In parallel with the theoretical effort, comprehensive series of model experiments have been undertaken against which code performance can be measured.

CEA/DRNR Cadarache has been involved in the MARA series of experiments /1/, consisting of, to date, nine 1/30th scale containment tests in Super Phénix geometry. Early tests in the series comprised simple bare tank configurations, but then progressively more complex tests were performed with internal components added step by step. The effects of a deforming roof are also considered /2/.

Analysis of the tests has been undertaken using SIRIUS /3/, and CASSIOPEE /4/, and, for MARA-01, SEURBNUK /5/, and ASTARTE /6/, calculations have also been performed. This broader based comparison is here extended to the MARA-04 test.

### 2. THE MARA-04 EXPERIMENT

A schematic of the experimental rig is given in Figure 1. The test comprises a roof-supported cylindrical tank with a torospherical base, partially filled with water and enclosing a 45gm spherical charge situated on the axis of symmetry slightly above the mid-height level. Surrounding the charge some details of the reactor core geometry are simulated including a diagrid, core support structure, and inner tank which extends upwards from the

---

\* A.Zucchini performed the CASSIOPEE calculation on attachment duty at CEN/DRNR Cadarache.

top of the core support, then outwards towards the outer vessel via a conical redan. At its outer extremity the redan is not attached to the main vessel but to a close-fitting cylindrical sleeve (see inset to Fig 1) which extends up to the roof level. The sleeve, which is free at its upper rim, slides freely on the inner surface of the main vessel.

The roof is notionally rigid with an annular cavity machined into the underside to compensate by volume for extra expansion spaces above the sodium level in the reactor. The core support structure is machined from a single block of Au 4g aluminium. All other internals are made from AISI 304L stainless steel with the main vessel itself of AISI 316 stainless steel, cold worked around the curved base.

The test is well instrumented with 11 strain gauges, axial and circumferential, and 14 pressure transducers, 4 within the fluid and 10 measuring roof loadings. In addition, as a visual aid, high speed photography was used during the test.

### 3. MATERIAL PROPERTIES

The thickness variations around the curved base resulting from the cold working during manufacture have been carefully measured and hardness tests performed on test specimens cut from a similar tank. Accordingly, for the calculations, the vessel is divided into 4 zones around the curved base and a further zone for the unworked cylindrical section, as indicated in Figure 2. Different static stress-strain data are specified for each zone appropriate to the degree of work hardening ascertained.

Strain rate effects are taken into account by applying a correction factor to the stress-strain curves for each zone, so that

$$\sigma_D = \sigma_S \left[ 1 + \frac{\dot{\epsilon}}{k_1} \right]^{k_2} \quad (1)$$

where  $\sigma_S$ ,  $\sigma_D$  refer respectively to the static and dynamic stresses, and  $\dot{\epsilon}$  the uniaxial strain rate. The factors  $k_1(\epsilon)$ ,  $k_2(\epsilon)$  are appropriate functions of strain determined empirically using results from a series of dynamic tensile tests.

For the CASSIOPEE calculation, the constitutive laws for the various structures are introduced in the analytic form (1) so that the "dynamic" correction is applied logically at each time step. In SEURBNUK-EURDYN a simpler procedure is adopted in which the material laws are specified in terms of a tri-linear stress-strain relation derived from (1) for an appropriate averaged strain rate. Typical strain rates for the deforming structures in MARA-04 are indicated in Figure 2.

Interpretation of the charge calibration tests carried out as part of the MANON series of experiments /7/, changes with the new "dynamic" material properties. This has led to a re-examination of the results from the tests and a new "dynamic" equation of state for the charge bubble derived, consistent with the new data. The new bubble law is adopted for the dynamic calculations performed in this study.

### 4. THE COMPUTER MODELS

The computational techniques and modelling capabilities of the four codes vary considerably but are representative of the diversity of approaches in common usage in containment analysis. A summary of the major code characteristics is given in Table I. Note that the version of

SEURBNUK coupled to the structures code EURDYN /8/, is used here in order to model realistically details of the core support structure.

All codes incorporate finite difference discretisations for the fluid, implicit in SEURBNUK-EURDYN, explicit for the other codes, and all adopt an explicit time integration procedure for the structure calculation. Each code is 2D axisymmetric.

In SEURBNUK-EURDYN plane-strain triangular elements are used for modelling the core support, while SIRIUS and CASSIOPEE use quadrilateral continuum elements. These differences are not significant because of the global strength of the structure. All other structures are modelled using thin shell theory.

CASSIOPEE uses Lagrange and Euler domains for the fluid as indicated in Figure 3, with the Euler description preferred for the region of greatest relative shear. Notice the similarity between the upper boundary of the Euler domain and the surface of separation between the radial and axial meshes in SIRIUS. In SEURBNUK-EURDYN a finer mesh structure is adopted than for the other codes; the Eulerian prescription in the code requires good resolution around the spherical charge bubble during the early stages of the calculation. The fine mesh also assists the code logic around the angles of the core support.

None of the codes model explicitly the annular cavity in the roof. Rather, the roof lower boundary is considered flush with the water surface and the equation of state of the air gap modified accordingly:

$$P = P_0 \left\{ \frac{V_0 + V_c}{V + V_c} \right\}^\gamma - P_0 \quad (2)$$

in which  $V_0$  is the initial (excluding cavity) volume of air,  $V_c$  the volume of the cavity region ( $5000\text{cm}^3$ ), and  $P_0$  the normalisation pressure (1 bar). The maximum air pressure will then be 7.7 bars, corresponding to compression of the air into the cavity space.

In the MARA-04 test the diagrid plate rests under gravity on the inner flange of the core support, there being no other attachment. As a result of fluid pressurisation on the upper surface during the transient, the diagrid bends downwards and will slide tangentially on its support near the rim, see Figure 4a. Only in CASSIOPEE is the support condition modelled realistically. For SIRIUS and SEURBNUK-EURDYN a hinged support is used instead. The consequences of this approximation are discussed in Section 4.

In SIRIUS and SEURBNUK-EURDYN the sleeve section of the inner tank is merged with the main vessel, the thickness of which is increased appropriately. To simulate the free slide condition of the sleeve, the redan is joined to the main vessel by a false shell element of negligible strength. In CASSIOPEE the sleeve is modelled as a separate shell free to slide on the main vessel, but not to detach from it. A weak element is used to couple the redan to the sleeve. Figure 4a suggests that during the experiment the sleeve slipped longitudinally and pulled away inwards from the main vessel. This behaviour is not adequately represented by any of the code simulations.

## 5. RESULTS AND COMPARISONS

Calculations were taken to 5 msec into the transient, by which time the major loading events were complete and the structures had reached, or were oscillating about, final rest

positions. The outlines shown in Figure 4 are drawn from final mesh configurations, and these are compared to experiment. The only discernible point of discrepancy is that each code predicts rounding of the joint between the cylindrical and conical sections of the inner tank, a feature not seen in the experiment.

A summary of other code comparisons is given in Table II. CASSIOPEE and SEURBNUK-EURDYN results are taken from calculations with "dynamic" materials data. SIRIUS and ASTARTE /9/, use "static" data. The main difference appears in the energy release from the charge bubble, which is 30% higher in the "dynamic" case.

Slug impact occurs at the roof centre at the time given in the Table. The integrated roof impulses are lower in SIRIUS as a consequence of the reduced charge energy.

Diagrid deflection depends critically on the coupling condition at the rim. The simple support used in CASSIOPEE yields good predictions, while the hinge condition used in SEURBNUK-EURDYN unrealistically adds membrane strength to the diagrid reducing the deflection by half. Nevertheless, the total displacement is in good agreement. In ASTARTE the core support cannot move, and in SIRIUS the movement is underestimated. This enhances the diagrid deflection compensating for the hinge constraint.

Inner tank strains are reasonable given that the magnitudes are outside the domain of the small strain theory used in the shell models. Main vessel strains are adequately predicted, showing no obvious anomalies, and no clear improvements due to the inclusion of strain-rate dependent material models.

## 6. CONCLUSIONS

Specific conclusions to be drawn from the exercise are:

- (1) Code predictions are in overall good agreement with measured values.
- (2) Strain-rate dependent material properties are important in the calibration tests for the charge, this significantly affecting roof impulses, but is of minor consequence otherwise.
- (3) There are no discernible effects due to differences in numerical approach. Much more important is an adequate representation of the structure boundary conditions.

Finally, it is worth remarking that although complex experiments like MARA-04, containing linked structures, are a good test of overall code performance, it is not always possible to trace origin of a particular point of discrepancy. Much simpler tests are better suited for this.

## 7. REFERENCES

- /1/ BLANCHET, Y. et al "Validation of the Containment Code SIRIUS: Interpretation of an Explosion Experiment on a Scale Model", Proc. Int. Meeting on Fast Reactor Tech., Seattle (1979).
- /2/ FICHE, C. et al "Theoretical-Experimental Study of Flexible Roof Effects in an HCDA Simulation", Paper E4/5, SMIRT-8, Brussels (1985).
- /3/ BLANCHET, Y. OBRY, P. LOUVET, J. "Treatment of Fluid-Structure Interaction with the SIRIUS Computer Code", Paper B6/8, SMIRT-6, Paris (1981).

- /4/ GRAVELEAU, J. LOUVET, P. "Calculation of Fluid-Structure Interaction for Reactor Safety with the CASSIOPEE Code", Paper B1/7, SMiRT-5, Berlin (1979).
- /5/ ACKER, D. et al "MARA 01/02 - Experimental Validation of the SEURBNUK and SIRIUS Containment Codes", Paper E3/6, SMiRT-6, Paris (1981).
- /6/ DANIERI, A. et al "Influence of the Representation Models of the Stress-Strain Law on the LMFBR Structures in an HCDA", Paper E4/4, SMiRT-6, Paris (1981).
- /7/ DAVID, F. et al "Etude d'une Composition Explosive Flegmatisée - Application à la Déformation d'une Cuve", Proc. Symp. Hautes Press. Dyn., Paris (1978).
- /8/ SMITH, B.L. YERKES, A. ADAMSON, J. "Status of the Coupled Fluid-Structure Dynamics Code SEURBNUK", Paper B9/1, SMiRT-7, Chicago (1983).
- /9/ CIGARINI, A. DANIERI, A. TOSELLI, G. "Applications of ASTARTE-4 Code to Explosive Models with Complex Internal Structure Using the Rezoning Facility", Paper B9/3, SMiRT-7, Chicago (1983).

Table I

A Comparison of Code Characteristics

DESCRIPTION	SEURBNUK- EURDYN	SIRIUS	CASSIOPEE	ASTARTE
Fluid Mesh	Euler	Lagrange	Euler/ Lagrange	Lagrange
Fluid Discretisation	F.Diff.	F.Diff.	F.Diff.	F.Diff.
Structure { Shell Discretisation { Continuum	F.Elem. F.Elem.	F.Elem. F.Diff.	F.Diff. F.Diff.	F.Diff. F.Diff.
Time { Fluid Integration { Structure	Implicit Explicit	Explicit Explicit	Explicit Explicit	Explicit Explicit
Subcycling	Yes	No	Yes	No

Table II

A Comparison of Results with Experiment

	CASSIOPEE	SEURBNUK - EURDYN	SIRIUS	ASTARTE	EXPERIMENT
Material Laws	Dynamic	Dynamic	Static	Static	
Time to Roof Impact (msec)	1.8	1.7	1.8	1.8	1.7
Roof Impulse (KPa-sec)	7.1	6.2	4.6	NA	6.6
Diagrid Central Displacement (mm) { Max Final	48.1 37.2	34.3 19.0	NA 26.8	21.6 20.6	NA 32.0
Diagrid Central Deflection (mm) { Max Final	23.0 22.0	11.0 8.5	17.3 15.9	21.6 20.6	NA 16.7
Vessel Base Displacement (mm) { Max Final	33.9 26.8	32.3 24.5	24.5 19.5	25.5 12.0	38.6 30.9
Hoop Strain Inner Tank (%) { Max Final	13.4 12.6	9.7 9.2	8.3 8.3	12.3 6.0	NA 12.0
Hoop Strain Lower Bulge (%) { Max Final	2.9 2.9	2.9 2.7	2.2 2.2	3.5 3.4	3.5 3.2
Hoop Strain Upper Bulge (%) { Max Final	4.4 4.2	4.2 3.9	3.0 3.0	5.1 5.1	3.6 3.6

NA - Not Available

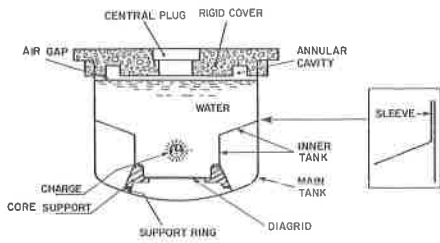


Figure 1 MARA-04 Experimental Arrangement

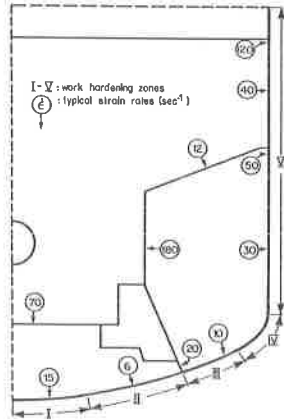


Figure 2 Work Hardening Regions and Strain-Rate Distribution

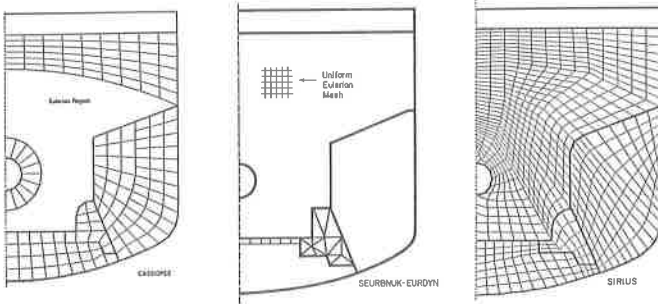


Figure 3 Initial Mesh Configurations - (a) CASSIOPEE  
(b) SEURBNUK-EURDYN  
(c) SIRIUS

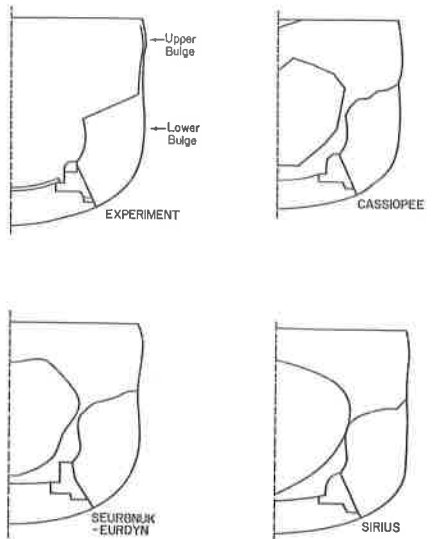


Figure 4 Final Displacements -  
(a) Measured  
(b) CASSIOPEE Calculation  
(c) SEURBNUK-EURDYN Calculation  
(d) SIRIUS Calculation